Article

Not peer-reviewed version

Performance Analysis Of Electric Vehicles With Fuel Cell-Supercapacitor Hybrid System

Carlos Armenta-Déu * and Alejandro Arenas

Posted Date: 21 June 2023

doi: 10.20944/preprints202306.1466.v1

Keywords: Electric Vehicle; Fuel Cell; Supercapacitor; Hybrid Power System; Energy Efficiency Improvement; Energy Reduction; Power System Management; Optimization

Article

Performance Analysis Of Electric Vehicles With Fuel Cell-Supercapacitor Hybrid System

Carlos Armenta-Déu * and Alejandro Arenas

Universidad Complutense de Madrid, Madrid, Spain

Abstract: This paper presents a new methodology to evaluate the performance of an electric vehicle hybrid power system consisting of a fuel cell and a supercapacitor. The study compares the results with those obtained for a battery-electric vehicle. The methodology extends to three driving modes, ECO, NORMAL, and SPORT, corresponding to conservative, moderate, and aggressive acceleration, and three driving conditions, low, medium, and high energy demand. We develop a simulation process to evaluate the energy consumption and the energy rate of a specific electric vehicle used as a prototype for the study. The methodology applies to a driving route that includes acceleration, deceleration, braking, and constant speed segments reproducing standard driving conditions in urban journeys. The proposed method considers combined driving modes, ECO, NORMAL, and SPORT, in each acceleration process, with variable fractions, 0% to 100%, for each mode. This methodology optimizes the simulation results as it fits the current driving way in urban environments. The simulation results show an average reduction in energy consumption of 37% and 27.1% in vehicle weight, contributing to lower energy use. The study concludes that using a hybrid power system, fuel cell/supercapacitor, instead of a battery in electric vehicles is beneficial, especially in journeys with frequent acceleration processes.

Keywords: electric vehicle; fuel cell; supercapacitor; hybrid power system; energy efficiency improvement; energy reduction; power system management; optimization

Introduction

The electric vehicle represents today the alternative to engine combustion cars in the search for a cleaner environment. The electric vehicle industry mainly operates with electric batteries to propel EVs; however, the problems associated with the scarcity of lithium, the main component of electric vehicle batteries [1–4], which may limit the use of battery electric vehicles [5–7], forced the manufacturers to search for an alternative propelling system, hydrogen [8–12].

The development of hydrogen fuel cell electric vehicles (HFCEVs) is a pending task to implement this kind of transportation in the modern society [13,14]. The low specific power of fuel cells is the main problem that arise when using hydrogen cells in electric vehicles [15,16]. Consequently, fuel cells cannot power electric vehicles in high demanding power periods because of the dynamics of hydrogen cell operation, using batteries to power the vehicle [17,18]. Battery vehicles are more capable, but the high current supply leads to high discharge rate, which affect the driving range [19–22].

The hydrogen system is lighter than batteries needed to propel a vehicle; however, the acceleration capacity decreases. To reduce this effect, we can use supercapacitors, which operate like batteries but with much higher charge and discharge capacity, weighing much less than a battery bank and playing the role of a power boost [23–25].

In this work, we simulate the performance of electric vehicles equipped with a hybrid system made up of a fuel cell and a supercapacitor, determining the gain in the driving range compared to the single fuel cell system.

Fuel cell Electric Vehicle (FCEV)

Preprints (www.preprints.org) | NOT PEER-REVIEWED | Posted: 21 June 2023 doi:10.20944/preprints202306.1466.v1

The basic structure of a fuel cell power system in an electric vehicle consists of a series and parallel fuel cell grouping to generate the required voltage and current to supply power to the electric motor. Figure 1 shows the schematic layout of the fuel cell power system in an electric vehicle.

The global voltage of the Fuel Cell system is determined using the following equation:

$$V_{FC} = N_s \left(V_r - \Delta V_{act} - \Delta V_{ohm} - \Delta V_{conc} \right) \qquad (1)$$

N_s is the number of serial fuel cells, Vr is the reversible voltage of the fuel cell, and ΔV is the voltage drop [26]. Sub-indexes *act*, *ohm*, and *conc* account for the activation process of chemical species [27–29], ohmic losses due to ionic and contact resistance [30], and concentration effects caused by mass transportation [31,32].

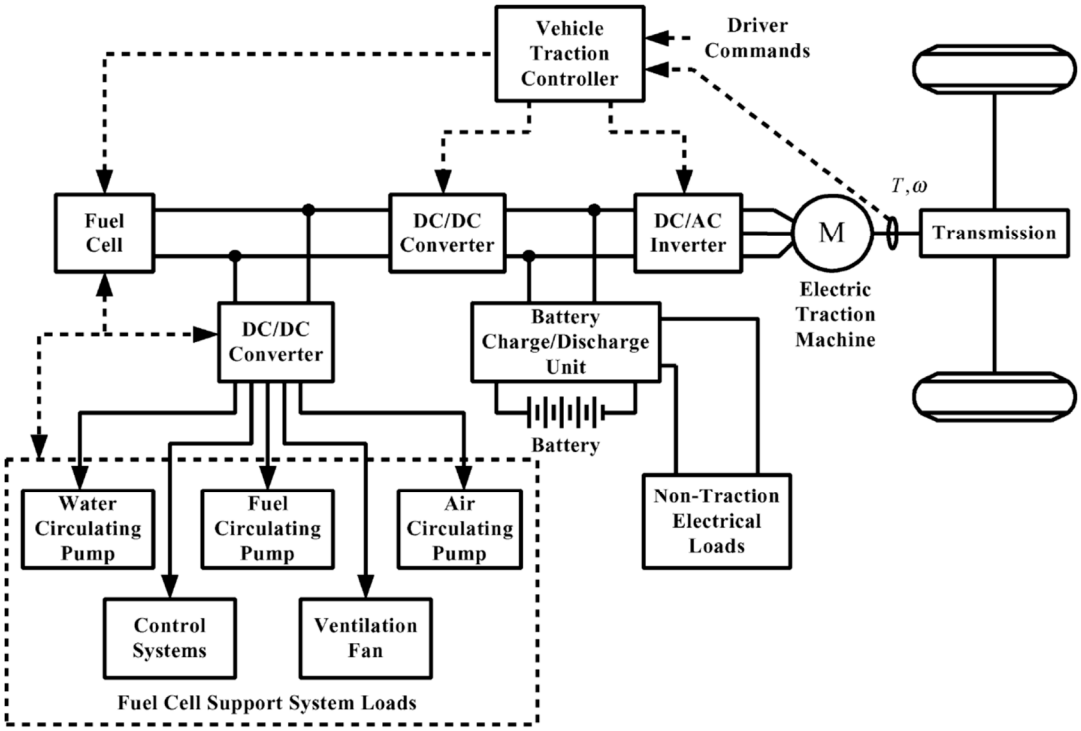

Figure 1. Schematic view of a Fuel Cell System for Electric Vehicles.

The total current generated by a group of fuel cells depends on the hydrogen flow according to the process:

$$I_{FC} = 2N_p e^- \frac{\rho_{H_2} \dot{V}_{H_2}}{M_{H_2}} \qquad (2)$$

Np is the number of parallel cells of the fuel cell system, *e-* is the electron electric charge, and ρ, *M*, and V are the density, molecular weight, and hydrogen flow, respectively.

Combining equations 1 and 2:

$$P_{FC} = 2N_s N_p \left[\left(V_r - \Delta V_{act} - \Delta V_{ohm} - \Delta V_{conc} \right) \right] e^- \frac{\rho_{H_2} \dot{V}_{H_2}}{M_{H_2}} = \qquad (3)$$

$$= 2N_s N_p \left(V_r - \Delta V \right) e^- \frac{\rho_{H_2} \dot{V}_{H_2}}{M_{H_2}}$$

Considering that the reversible fuel cell voltage and the voltage drop, ΔV, are constant:

Preprints (www.preprints.org) | NOT PEER-REVIEWED | Posted: 21 June 2023 doi:10.20944/preprints202306.1466.v1

$$P_{FC} = C_{H_2} \dot{V}_{H_2} \qquad (4)$$

Where the constant C_{H2} is:

$$C_{H_2} = 2N_s N_p \left(V_r - \Delta V\right) e^{-} \frac{\rho_{H_2}}{M_{H_2}} \qquad (5)$$

Supercapacitor

We may find three types of supercapacitors, electrochemical double-layer capacitors (EDLC), pseudo-condensers, and hybrid condensers [33–35]. The working mechanism of a supercapacitor is faradaic, non-faradaic, and a combination of both [36–41]. Faradaic supercapacitors characterize by electric charge transfer between electrode and electrolyte; however, in the non-faradaic type, there is no chemical reaction but a charge redistribution due to physical processes [42].

EDLC supercapacitors, used in high-density storage systems, are known as ultra-condensers and derive from classical condensers [43]. Nevertheless, the storage capacity of an EDLC is of farads, but in classical condensers is only of micro or mini-farads [44]. The greater storage capacity of an EDLC is due to its electrode/electrolyte electrochemical structure since the storage is in ionic form, which allows it to deliver high power. Indeed, the porous structure of the electrode increases the storage surface, and the charge density, which combined with a longer charge exchanging time, produces higher storage capacity.

Due to the higher storage capacity, the electric vehicle industry uses EDLC for regenerative braking and acceleration processes as an alternative to batteries [45]. The quick charge/discharge process in EDLC reduces the energy losses and increases the efficiency [46].

Performance Simulation

To run the simulation, we design a prototype representing the main characteristics of a different electric vehicle model selection. We replace the batteries of the prototype with a hybrid fuel cell and supercapacitor unit. The simulation run applies to three scenarios, high, medium, and low energy-demanding routes, corresponding to the three types of driving according to the drivers' attitude, aggressive, moderate, and conservative mode. An acceleration of 2.75 m/s^2, 1.75 m/s^2, and 1.25 m/s^2 characterizes the three driving modes, respectively.

The driving conditions for the simulation running correspond to the different processes included in urban routes, acceleration, deceleration, constant speed, and braking. These processes occur with a non-defined sequence in a daily urban route; therefore, to simplify the calculation, we grouped all segments corresponding to the same process independently of the time they occur. Nevertheless, since the driving conditions at which the process takes place are not the same, for instance, different initial and final speeds or variations in the slope of the route, we divided every process into segments that share the same driving conditions. Tables 1–3 show the result of this classification.

Table 1. Characteristics of the route for the simulation (low demanding).

Slope (º)	Initial speed (km/h)	Final speed (km/h)	Number of segments	Driving condition
-1	0	60	4	Acceleration
	60	60	1	Constant speed
	60	70	3	Acceleration
	70	70	1	Constant speed
	70	60	3	Deceleration
	60	0	7	Braking
	0	50	5	Acceleration
	50	50	10	Constant speed

Preprints (www.preprints.org) | NOT PEER-REVIEWED | Posted: 21 June 2023 doi:10.20944/preprints202306.1466.v1

0	50	90	4	Acceleration
	90	90	2	Constant speed
	90	50	4	Deceleration
	50	0	9	Braking
1	0	50	5	Acceleration
	50	50	3	Constant speed
	50	80	4	Acceleration
	80	80	5	Constant speed
	80	50	4	Deceleration
	50	0	9	Braking

Table 2. Characteristics of the route for the simulation (medium demanding).

Slope (º)	Initial speed (km/h)	Final speed (km/h)	Number of segments	Driving condition
-3	0	60	4	Acceleration
	60	60	1	Constant speed
	60	70	3	Acceleration
	70	70	1	Constant speed
	70	60	3	Deceleration
	60	0	7	Braking
0	0	50	5	Acceleration
	50	50	10	Constant speed
	50	90	4	Acceleration
	90	90	2	Constant speed
	90	50	4	Deceleration
	50	0	9	Braking
3	0	50	5	Acceleration
	50	50	3	Constant speed
	50	80	4	Acceleration
	80	80	5	Constant speed
	80	50	4	Deceleration
	50	0	9	Braking

Table 3. Characteristics of the route for the simulation (high demanding).

Slope (º)	Initial speed (km/h)	Final speed (km/h)	Number of segments	Driving condition
-5	0	60	4	Acceleration
	60	60	1	Constant speed
	60	70	3	Acceleration
	70	70	1	Constant speed
	70	60	3	Deceleration
	60	0	7	Braking
0	0	50	5	Acceleration
	50	50	10	Constant speed
	50	90	4	Acceleration
	90	90	2	Constant speed
	90	50	4	Deceleration
	50	0	9	Braking
	0	50	5	Acceleration
	50	50	3	Constant speed
	50	80	4	Acceleration

Preprints (www.preprints.org) | NOT PEER-REVIEWED | Posted: 21 June 2023 doi:10.20944/preprints202306.1466.v1

5	80	80	5	Constant speed
	80	50	4	Deceleration
	50	0	9	Braking

The driven distance for every case is 8.17 km for a global driving time of 0.2 hours.

The simulation considers that the acceleration is not constant in all cases since the driver may accelerate the electric vehicle differently during a segment; therefore, we divided each acceleration process into three, 30% of the time accelerating at conservative mode (ECO mode), 60% at moderate acceleration (NORMAL mode), and 10% at aggressive acceleration (SPORT mode).

The simulation also calculates the charge consumption, in *Ah/km*, and the hydrogen flow required for every segment. The calculation method is the same as the one applied to electric vehicles equipped with batteries.

Today, we find few commercial electric vehicles equipped with fuel cells; therefore, to obtain a valid result from the simulation process, we take the Hyundai NEXO as a reference, with a reported hydrogen consumption rate of 0.95 kg/100 km [47]. We use previous results as a reference for the process efficiency [48], adapting the results to a lighter and less powerful electric vehicle (Figure 2).

Figure 2 extends the analysis of the fuel cell power up to 300 kW, which corresponds to a heavy truck; however, in our case we establish the limit in 70.15 kW, corresponding to a light vehicle (red dotted line).

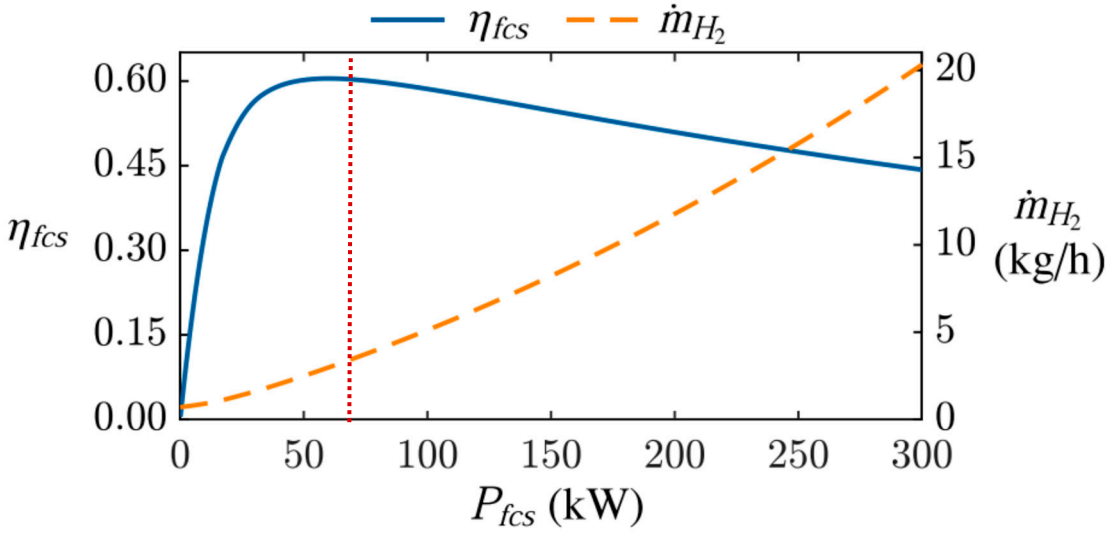

Figure 2. Efficiency and hydrogen consumption rate for a Fuel Cell Electric Vehicle.

If we adapt the efficiency curve in Figure 2 to the prototype tested in our case, we obtain (Figure 3):

Preprints (www.preprints.org) | NOT PEER-REVIEWED | Posted: 21 June 2023 doi:10.20944/preprints202306.1466.v1

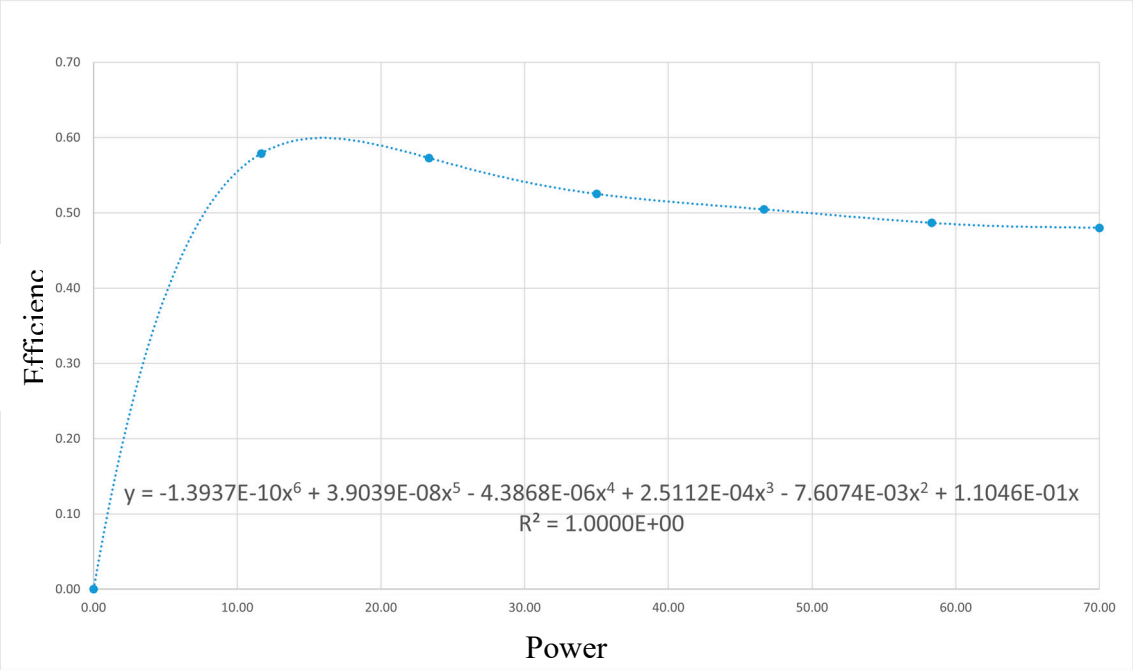

Figure 3. Efficiency of the prototype Fuel Cell (simulation results).

The algorithm inserted in Figure 3 shows the polynomial function that fits the calculated efficiency of the simulated fuel cell. We notice the perfect fitting between theoretical calculation and correlation fit.

The efficiency allows the technician or user to determine the fuel consumption through the required energy for every segment.

Technical Data

To run the simulation we use specific technical data for the fuel cell/supercapacitor hybrid system. Table 4 shows the main parameters of the battery that powers the electric vehicle.

Table 4. Values of the battery main parameters for the simulation process.

Parameter	Value
Front area (A)	2.5
Aerodynamic coefficient (C_x)	0.3
Rolling coefficient (μ)	0.03
Air density (ϱ)	1.225
Discharge efficiency (η_D)	0.85
Regenerative process energy efficiency (η_r)	0.70
Vehicle mass (kg)	1000
Battery voltage (V)	400
Maximum power (kW)	150

The vehicle mass corresponds to the curb weight without a powertrain, battery, or fuel cell/supercapacitor hybrid system. The efficiencies, discharge and regenerative braking correspond to the battery discharge (wheel to the battery) and charge (battery to wheel) efficiency, which currently depend on temperature and driving mode; however, in our case, we consider these parameters constant for the simulation run. The selected efficiencies correspond to the Nissan LEAF model; A. Boretti [49] reports wheel-to-battery and battery-to-wheel efficiencies for the Nissan LEAF within the range of 30%-79% and 55.3%-89.6%. We adopted representative values within the intervals based on statistical studies [50,51]. Nevertheless, since a battery and a supercapacitor do not have

Preprints (www.preprints.org) | NOT PEER-REVIEWED | Posted: 21 June 2023 doi:10.20944/preprints202306.1466.v1

identical performance, the charge/discharge cycling efficiency values are different; therefore, we use specific coefficients for each system at the simulation run.

According to the above statement, the parameter values used for the simulation in the case of supercapacitor are (Table 5):

Table 4. Values of the main parameters for the hybrid fuel cell/supercapacitor system (simulation process).

Parameter	Value
Front area (A)	2.5
Aerodynamic coefficient (C_x)	0.3
Rolling coefficient (μ)	0.03
Air density (ϱ)	1.225
Fuel Cell average efficiency (η_D)	0.55
Discharge efficiency (%)	0.80
Regenerative process energy efficiency (η_r)	0.90
Vehicle mass (kg)	1000
Operating voltage (V)	69
Supercapacitor maximum power (kW)	16
Fuel Cell maximum power (kW)	70.15
Hydrogen storage tank mass (kg)	85.71
Fuel Cell mass (kg)	56
Fuel Cell consumption rate (kg/100 km)	0.95
Supercapacitor capacitance (F)	130
Supercapacitor mass (kg)	14

In absence of enough technical data for the Hyundai NEXO, the prototype used for evaluation in the present study, we base our analysis on data taken from the Technical Data Sheet of Toyota MIRAI [52] and the webpage for Hyundai NEXO [47], which are electric vehicles of similar characteristics to the Hyundai NEXO.

Previous work [53] evaluated the supercapacitors' efficiency during the regenerative process, reporting values between 80% and 98%. We decided to apply intermediate data within the mentioned interval to operate under similar conditions in the case of the battery propelling system.

We calculate the hydrogen storage mass tank using the technical data provided for the Hyundai NEXO [54] and apply the data for the Toyota MIRAI technical characteristics, resulting in the values reported in Table 4 [55].

The supercapacitor used for the simulation run is the model XLM-69R0137A-R" from EATON [56] since it supplies maximum power compatibility to the required value in the simulation.

Energy Evaluation

To calculate the energy consumption by the electric vehicle in every step of the route, we apply the dynamic equations to the driving conditions and the driving mode according to the drivers' attitude; the calculation procedure comes from previous work from one of the authors [57–62].

Mechanic required power derives from the dynamic driving conditions, and it is expressed by:

$$P_{mech} = F_T / v_{av} \qquad (6)$$

v_{av} is the average value of the vehicle speed, and F_T represents the total mechanical force, which obtained from:

$$F_T = ma + \frac{1}{2} C_x A \rho v_{av}^2 + g \mu m \cos\alpha \qquad (7)$$

The mass m accounts for the vehicle and power system mass, battery, or hybrid system. The parameter a represents the vehicle acceleration, and α is the slope of the route.

Preprints (www.preprints.org) | NOT PEER-REVIEWED | Posted: 21 June 2023 doi:10.20944/preprints202306.1466.v1

Because the electric motor does not operate at full efficiency mode:

$$P_{el} = P_{mech}\eta_{el} \quad (8)$$

P and η are the power and efficiency of the electric motor.

The battery capacity, C_{bat}, depends on the required energy to cover the expected driving range;

$$C_{bat} = \sum_i (P_{el}t)_i \quad (9)$$

Where i is the number of segments included in the driving range.

Combining equations 6 thru 9:

$$C_{bat} = \eta_{el}\sum_i \left[m\left(\frac{a}{v_{av}}\right)_i + \frac{1}{2}C_x A\rho(v_{av})_i + g\mu m\left(\frac{\cos\alpha}{v_{av}}\right)_i \right] t_i \quad (10)$$

Considering the acceleration process develops uniformly:

$$C_{bat} = \eta_{el}\sum_i \left[2m\left(1-\frac{v_{av}}{v_{in}}\right)_i + \frac{1}{2}C_x A\rho(v_{av})_i t_i + g\mu m\left(\frac{\cos\alpha}{v_{av}}\right)_i t_i \right] \quad (11)$$

The analysis of statistical data shows there is a relation between the capacity and the mass of an electric vehicle battery [63]:

$$m_{bat} = 9.0914C_{bat} + 0.033 \quad (12)$$

Because the vehicle mass depends on the battery mass:

$$m = m_{bat} + m_{EV} \quad (13)$$

Combining Equations 11, 12 and 13:

$$C_{bat} = \eta_{el}\sum_i \left[2\left([9.0914C_{bat}+0.033]+m_{EV}\right)\left(1-\frac{v_{av}}{v_{in}}\right)_i + \frac{1}{2}C_x A\rho(v_{av})_i t_i + g\mu\left([9.0914C_{bat}+0.033]+m_{EV}\right)\left(\frac{\cos\alpha}{v_{av}}\right)_i t_i \right] \quad (14)$$

Equation 14 is a recurrent function that forces the application of an iteration process to determine the battery capacity correct value.

Using the fuel cell and supercapacitor, we must adapt the vehicle to the hybrid system; following the same procedure as in the battery electric vehicle, we determine the required amount of hydrogen from:

$$n_{H_2} = \frac{W_{el}}{\eta Q_{H_2}} \quad (15)$$

Where n_{H_2} represents the mass of hydrogen, in moles, W_{el} is the electric work, Q_{H2} is the hydrogen combustion heat, and η is the combustion process efficiency.

Using the relation between mass and number of moles:

$$\frac{m_{H_2}}{M_{H_2}} = \frac{W_{el}}{\eta Q_{H_2}} \quad (16)$$

M_{H_2} is the hydrogen molecular weight.

In terms of power:

$$P_{el} = \dot{m}_{H_2}\eta\frac{Q_{H_2}}{M_{H_2}} \quad (17)$$

Which provides the relation between the electric power and the hydrogen mass flow.

The capacity of the supercapacitor is determined from the classical expression:

Preprints (www.preprints.org) | NOT PEER-REVIEWED | Posted: 21 June 2023 doi:10.20944/preprints202306.1466.v1

$$C_{SC} = 2\frac{P_{SC}}{V_o^2 - V_f^2}t \qquad (18)$$

P_{SC} is the power delivered by the supercapacitor, and V_o and V_f are the voltages of the supercapacitor at the fully charged and discharged state.

Equation 18 is only valid if $V_f \geq V_{min}$, where V_{min} is the minimum value of the supercapacitor voltage.

Simulation Results

The simulation looks for improving the management of the electric vehicle power supply system, a methodology previously used with good results [64]. One of the main goals of this simulation process is to optimize the performance of the electric vehicle power system to a more extend field of application than economics [65].

The simulation process includes the energy consumption calculation and power supply capacity. Additionally, we calculate the mass of the power source and electric vehicle to obtain the global weight. The simulation runs for the three defined scenarios, high, medium, and low demanding energy conditions, and for the three driving modes, aggressive (SPORT), moderate (NORMAL), and conservative (ECO), corresponding to high, medium, and low acceleration, respectively.

First group of simulations focuses on the electric vehicle equipped with a battery. Table 5 shows the results of the simulation.

Table 5. Results for the simulation of the battery electric vehicle performance.

Driving mode		Energy demanding level		
	Magnitude	Low	Medium	High
ECO	Charge consumption rate (Ah/km)	0.468	0.470	0.472
	Energy consumption rate (Wh/km)	187.316	188.090	188.760
	Charge consumption rate (Ah/100 km)	46.829	47.023	47.190
	Energy consumption rate (Wh/100 km)	18.732	18.809	18.876
	Capacity (Ah)	187.316	188.090	188.760
	Energy (kWh)	74.926	75.236	75.504
	Battery mass (kg)	549.594	551.315	552.802
NORMAL	Charge consumption rate (Ah/km)	0.569	0.571	0.573
	Energy consumption rate (Wh/km)	227.483	228.360	229.109
	Charge consumption rate (Ah/100 km)	56.871	57.090	57.277
	Energy consumption rate (Wh/100 km)	22.748	22.836	22.911
	Capacity (Ah)	227.483	228.360	229.109
	Energy (kWh)	90.993	91.344	91.644
	Battery mass (kg)	638.848	640.796	642.461
SPORT	Charge consumption rate (Ah/km)	0.587	0.589	0.591
	Energy consumption rate (Wh/km)	234.892	235.709	236.392
	Charge consumption rate (Ah/100 km)	58.723	58.927	59.098
	Energy consumption rate (Wh/100 km)	23.489	23.571	23.639
	Capacity (Ah)	234.892	235.709	236.392
	Energy (kWh)	93.597	94.284	94.557
	Battery mass (kg)	655.314	657.131	658.648

The comparative analysis of the simulation results for the three driving modes shows an increase in all the parameter values as we move from ECO to SPORT mode, in close agreement with what we expected. Table 6 shows the increasing ratio.

Preprints (www.preprints.org) | NOT PEER-REVIEWED | Posted: 21 June 2023 doi:10.20944/preprints202306.1466.v1

Table 6. Ratio of simulation values for the battery performance parameters.

NORMAL/ECO	SPORT/NORMAL	SPORT/ECO
1.214	1.032	1.254

To calculate the energy consumption, we consider that each acceleration process combines the three driving modes, ECO, NORMAL, and SPORT, at different proportions. The fraction in which each driving mode contributes may change; therefore, we selected all combinations provided the sum of the fractions equals one.

The car must meet the driving range requirement, so we used the highest battery capacity of the proposed scenarios, corresponding to the fastest acceleration. Analogously, the heaviest battery is selected to cover all cases and all accelerations.

We observe the SPORT and NORMAL mode have similar values with a slight difference of 3.2%. However, from ECO to NORMAL mode, the increase reaches 21.4% and 25.4% from ECO to SPORT; therefore, we may conclude that the ECO mode represents the most significant energy saving. Figures 4–6 show the results of the calculation for the three driving modes and driving conditions.

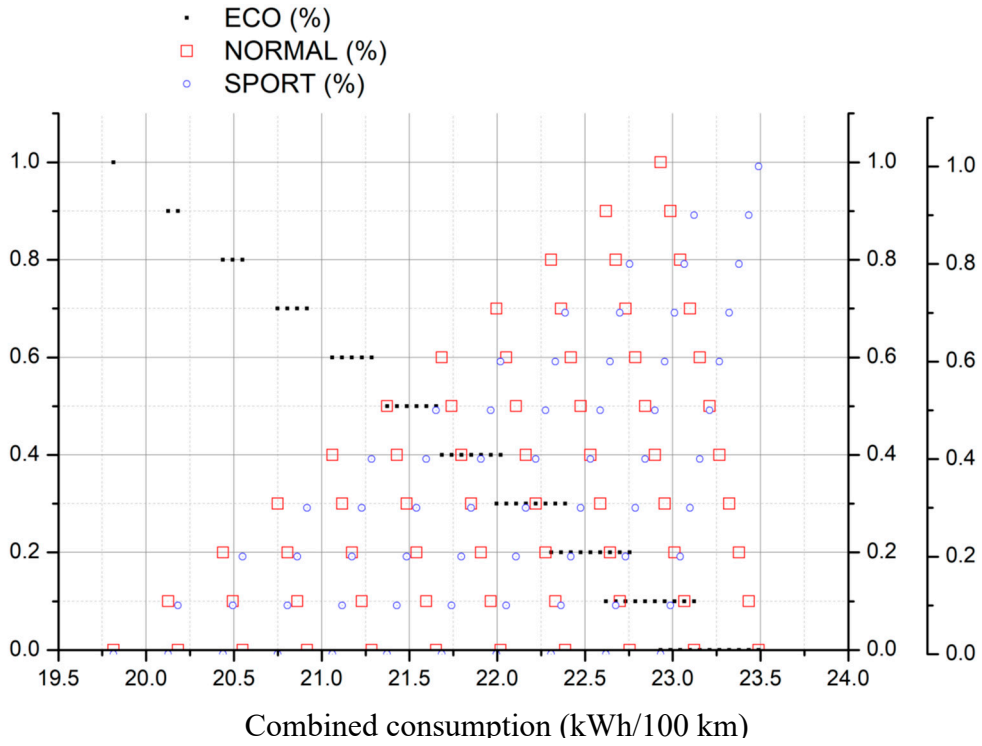

Figure 4. Combined consumption for low demanding energy rate in battery electric vehicles.

Preprints (www.preprints.org) | NOT PEER-REVIEWED | Posted: 21 June 2023 doi:10.20944/preprints202306.1466.v1

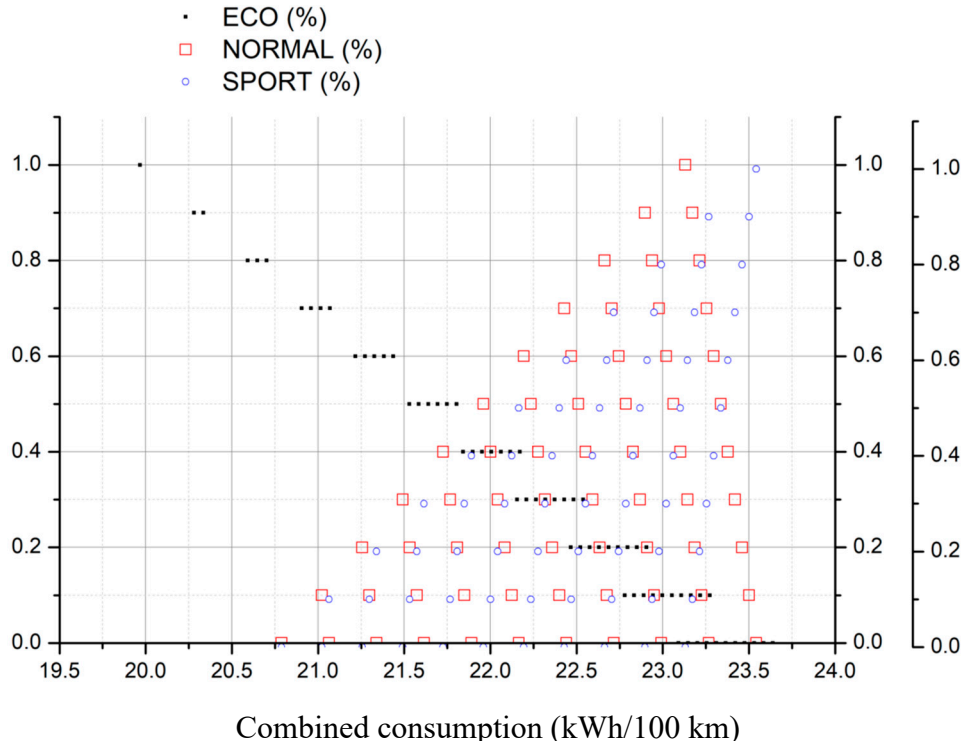

Figure 5. Combined consumption for medium demanding energy rate in battery electric vehicles.

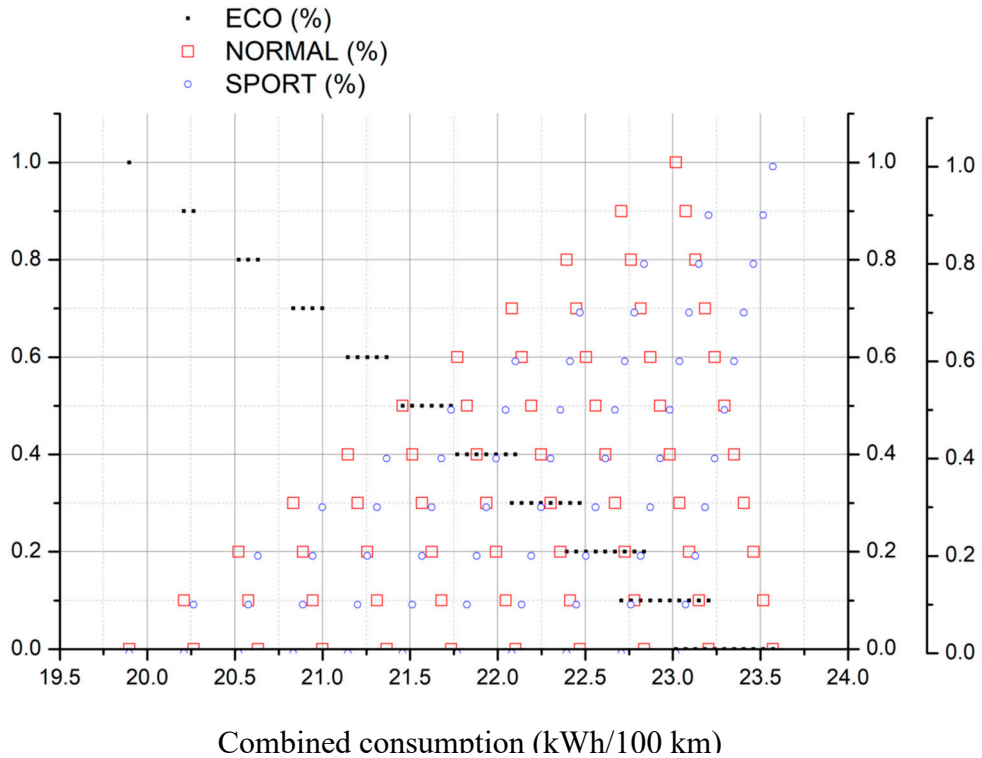

Figure 6. Combined consumption for high demanding energy rate in battery electric vehicles.

To determine the combined consumption using Figures 4–6 the user should operate in the following way:

a. Chose the type of demanding energy rate and select the corresponding figure

Preprints (www.preprints.org) | NOT PEER-REVIEWED | Posted: 21 June 2023 doi:10.20944/preprints202306.1466.v1

b. Select the fraction of conservative (ECO), moderate (NORMAL) and aggressive (SPORT) driving mode for the acceleration
c. Search for the selected values in the figure
d. Draw a vertical line downwards, joining all points of selected values until reaching the X-axis
e. The crossing point corresponds to the searched value

To automatize the process, we developed a control routine based on the algorithms that produce the results in Figures 4–6. Figure 7 shows the flowchart of the control routine.

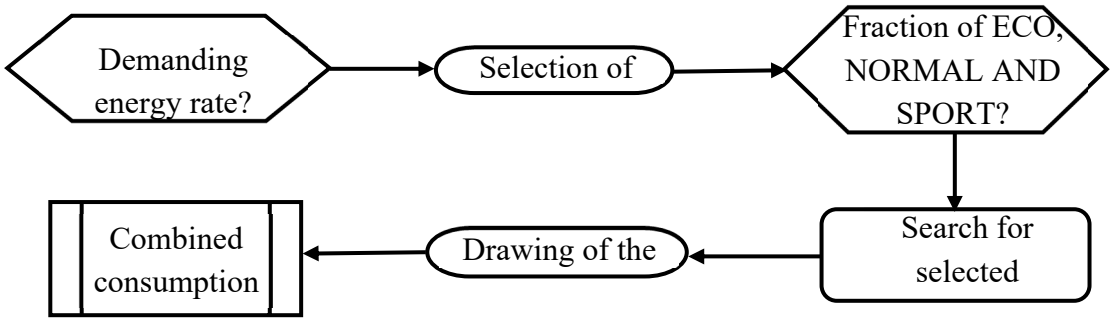

Figure 7. Flowchart of the control routine for combined consumption calculation.

The following example helps the user to operate manually using Figures 4–6.
Step 1
Control routine: *Demanding energy rate? ECO/NORMAL/SPORT*
User: *NORMAL*
Control routine selects Figure 5
Step 2
Control routine: *Fraction of ECO/NORMAL/SPORT acceleration?*
User: *0.5/0.3/0.2*
Control routine searches and marks selected points (black circles in Figure 8), then draws a right vertical line joining the circles (dotted black line in Figure 8). The crossing point with the X-axis determines the combined consumption (black rhombus).

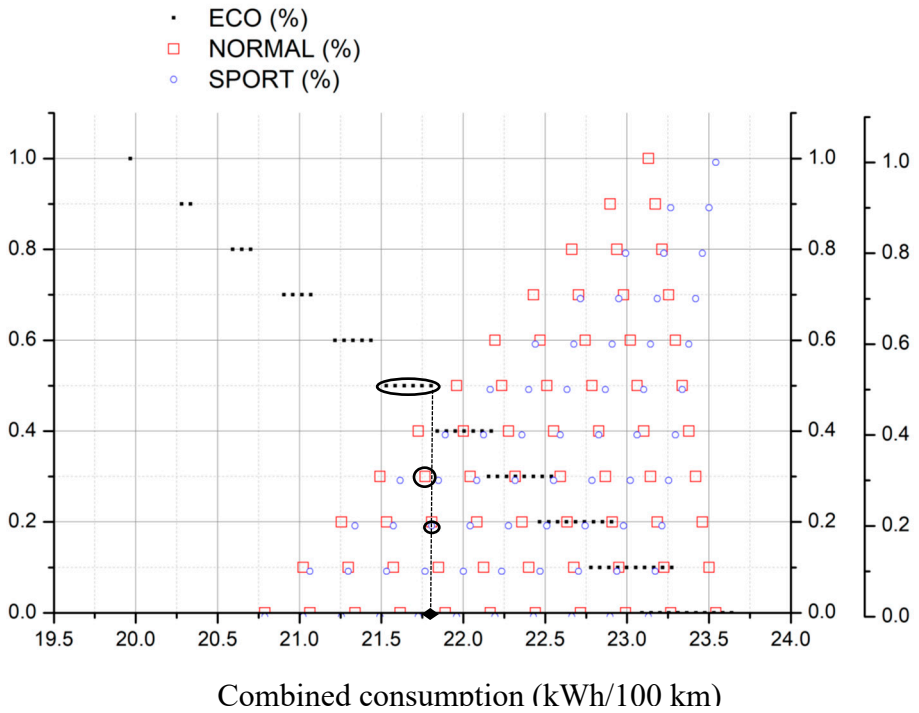

Preprints (www.preprints.org) | NOT PEER-REVIEWED | Posted: 21 June 2023 doi:10.20944/preprints202306.1466.v1

Figure 8. Operational mode to determine combined consumption for specific driving conditions (medium demanding rate) and modes in battery electric vehicles.

The second group of simulations deals with the electric vehicle equipped with the hybrid fuel cell and supercapacitor system. Table 7 shows the results of the simulation.

Table 7. Results for the simulation of the performance of the electric vehicle hybrid system.

Driving mode		Energy demanding level		
	Magnitude	Low	Medium	High
ECO	Energy consumption rate (Wh/km)	123.84	124.28	124.66
	Energy consumption rate (Wh/100 km)	12.38	12.43	12.47
	Hydrogen consumption (kg/100 km)	1.29	1.29	1.30
	Energy (kWh)	49.53	49.71	49.86
	Vehicle mass (kg)	1178	1178	1178
NORMAL	Energy consumption rate (Wh/km)	136.55	137.00	137.38
	Energy consumption rate (Wh/100 km)	13.66	13.70	13.79
	Hydrogen consumption (kg/100 km)	1.76	1.77	1.77
	Energy (kWh)	54.62	54.80	54.95
	Vehicle mass (kg)	1178	1178	1178
SPORT	Energy consumption rate (Wh/km)	148.11	148.56	148.95
	Energy consumption rate (Wh/100 km)	14.81	14.86	14.90
	Hydrogen consumption (kg/100 km)	2.87	2.87	2.88
	Energy (kWh)	59.24	59.42	59.58
	Vehicle mass (kg)	1178	1178	1178

In a similar way than for the battery electric vehicle, the comparative analysis of the simulation results for the three driving modes in the hybrid system electric vehicle shows an increase in all the parameter values as we move from ECO to SPORT mode, in close agreement with what we expected. Table 8 shows the increasing ratio.

Table 8. Ratio of simulation values for the battery performance parameters.

NORMAL/ECO	SPORT/NORMAL	SPORT/ECO
1.103	1.084	1.196
*1.214**	*1.032**	*1.254**

The data in italic mode correspond to the battery electric vehicle. We notice that the increasing rate reduces in all driving conditions concerning the battery electric vehicle, except for the NORMAL to SPORT case, which means that the acceleration effects are of lower importance in the case of a hybrid system due to the supercapacitor, which supports the acceleration processes. These results confirm the benefits of using a supercapacitor for acceleration instead of a battery.

Comparing data from Tables 5 and 7, we realize that there is a significant reduction in the energy and energy consumption rate for all driving modes. Table 9 shows the values of the comparative analysis.

Table 9. Comparative analysis of energy reduction between hybrid system and battery power supply for electric vehicles.

↓Magnitude	Driving mode →	ECO	NORMAL	SPORT
Energy (kWh)/Energy consumption rate (kWh/100 km)		34%	40%	37%

Preprints (www.preprints.org) | NOT PEER-REVIEWED | Posted: 21 June 2023 doi:10.20944/preprints202306.1466.v1

We observe that the reduction in energy consumption is 37%, on average, when using a hybrid fuel cell and supercapacitor system. This reduction is due to a higher performance of the hybrid system in the acceleration processes, where the supercapacitor supplies power to the electric vehicle.

Repeating the process of energy calculation for the hybrid fuel cell and supercapacitor system, using the developed algorithms, we obtain the energy consumption for the three driving modes and driving conditions (Figures 9–11).

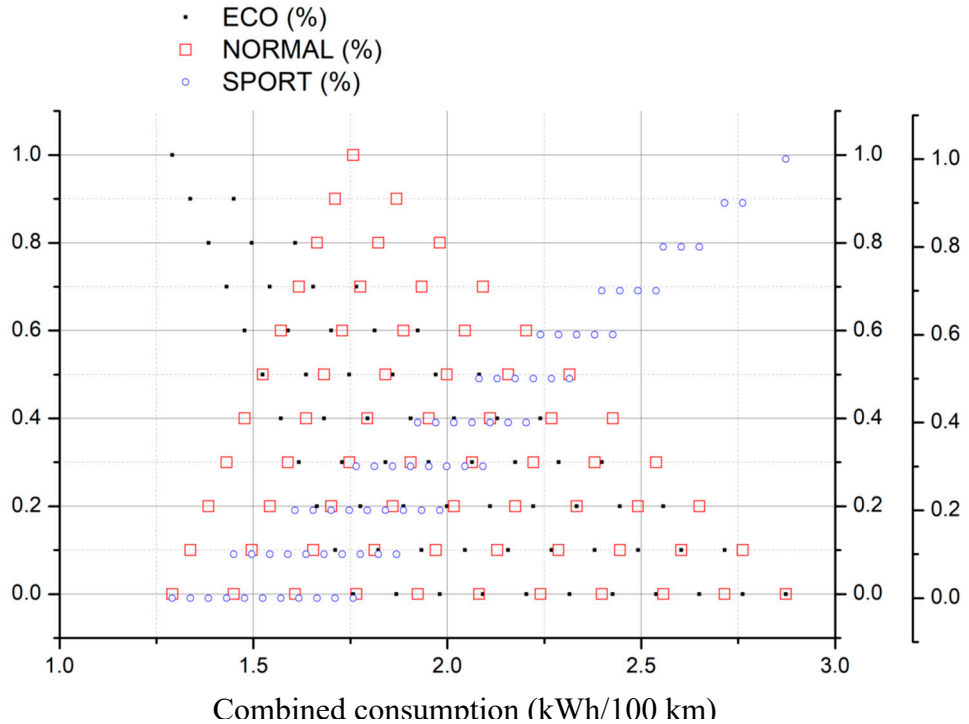

Figure 9. Combined consumption for low demanding rate of energy in electric vehicles with hybrid fuel cell and supercapacitor system.

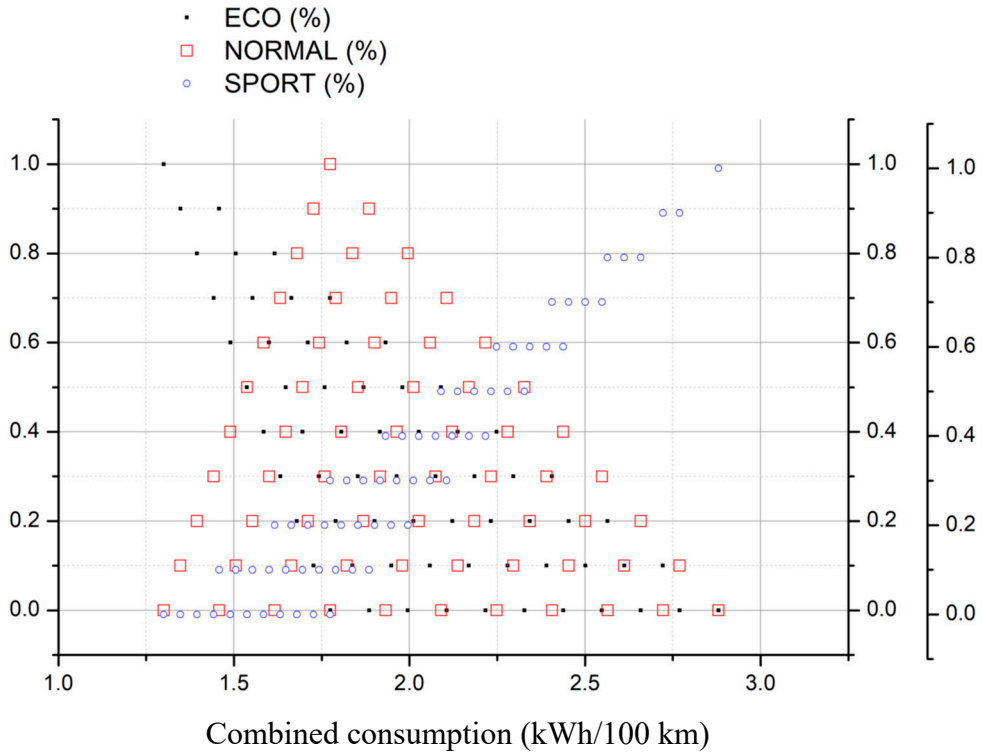

Preprints (www.preprints.org) | NOT PEER-REVIEWED | Posted: 21 June 2023 doi:10.20944/preprints202306.1466.v1

Figure 10. Combined consumption for medium demanding rate of energy in electric vehicles with hybrid fuel cell and supercapacitor system.

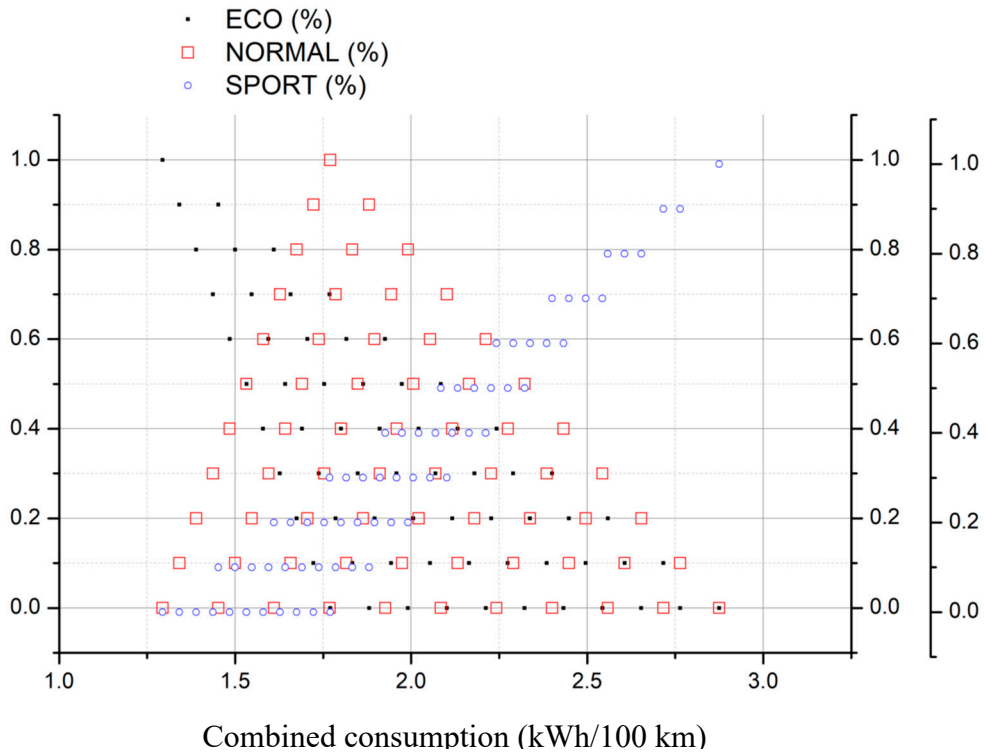

Figure 11. Combined consumption for high demanding rate of energy in electric vehicles with hybrid fuel cell and supercapacitor system.

Comparing the results obtained from the simulation process for the two tested power systems, battery and hybrid system, fuel cell, and supercapacitor, we can summarize that the average reduction when using the hybrid system is 37% in the power system capacity and 27.1% in the vehicle weight.

Conclusions

The use of supercapacitors for acceleration processes redounds in an improvement of the electric vehicle performance.

The combination of supercapacitor and fuel cell in a hybrid system to power electric vehicles represents a reduction in the capacity of the power supply and in the vehicle weight.

The average reduction of the energy consumption for a specific driving range, when using the hybrid system is 37%.

The replacement of the battery by the fuel cell/supercapacitor unit lowers the vehicle weight by 27.1%, which contributes to reduce energy consumption.

References

[1] Narins, T. P. (2017). The battery business: Lithium availability and the growth of the global electric car industry. *The Extractive Industries and Society*, *4*(2), 321-328.

[2] Sonoc, A., & Jeswiet, J. (2014). A review of lithium supply and demand and a preliminary investigation of a room temperature method to recycle lithium ion batteries to recover lithium and other materials. *Procedia Cirp*, *15*, 289-293.

[3] Egbue, O., & Long, S. (2012). Critical issues in the supply chain of lithium for electric vehicle batteries. *Engineering Management Journal*, *24*(3), 52-62.

[4] Wanger, T. C. (2011). The Lithium future—resources, recycling, and the environment. *Conservation Letters*, *4*(3), 202-206.
[5] Ljunggren Söderman, M., Kushnir, D., & Sandén, B. A. (2013). Will metal scarcity limit the use of electric vehicles?.
[6] Narins, T. P. (2017). The battery business: Lithium availability and the growth of the global electric car industry. *The Extractive Industries and Society*, *4*(2), 321-328.
[7] Liu, B., Zhang, Q., Liu, J., Hao, Y., Tang, Y., & Li, Y. (2022). The impacts of critical metal shortage on China's electric vehicle industry development and countermeasure policies. *Energy*, *248*, 123646.
[8] Thomas, C. E. (2009). Fuel cell and battery electric vehicles compared. *international journal of hydrogen energy*, *34*(15), 6005-6020.
[9] Contestabile, M., Offer, G. J., Slade, R., Jaeger, F., & Thoennes, M. (2011). Battery electric vehicles, hydrogen fuel cells and biofuels. Which will be the winner?. *Energy & Environmental Science*, *4*(10), 3754-3772.
[10] Wanitschke, A., & Hoffmann, S. (2020). Are battery electric vehicles the future? An uncertainty comparison with hydrogen and combustion engines. *Environmental Innovation and Societal Transitions*, *35*, 509-523.
[11] Bartolozzi, I., Rizzi, F., & Frey, M. (2013). Comparison between hydrogen and electric vehicles by life cycle assessment: A case study in Tuscany, Italy. *Applied energy*, *101*, 103-111.
[12] Wong, E. Y. C., Ho, D. C. K., So, S., Tsang, C. W., & Chan, E. M. H. (2021). Life cycle assessment of electric vehicles and hydrogen fuel cell vehicles using the greet model—A comparative study. *Sustainability*, *13*(9), 4872.
[13] Muthukumar, M., Rengarajan, N., Velliyangiri, B., Omprakas, M. A., Rohit, C. B., & Raja, U. K. (2021). The development of fuel cell electric vehicles–A review. *Materials Today: Proceedings*, *45*, 1181-1187.
[14] Yuan, Y., & Yuan, X. (2023). Does the development of fuel cell electric vehicles be reviving or recessional? Based on the patent analysis. *Energy*, *272*, 127104.
[15] Dixon, J. (2010, March). Energy storage for electric vehicles. In *2010 IEEE International Conference on Industrial Technology* (pp. 20-26). IEEE.
[16] Chau, K. T., Wong, Y. S., & Chan, C. C. (1999). An overview of energy sources for electric vehicles. *Energy Conversion and Management*, *40*(10), 1021-1039.
[17] Khaligh, A., & Li, Z. (2010). Battery, ultracapacitor, fuel cell, and hybrid energy storage systems for electric, hybrid electric, fuel cell, and plug-in hybrid electric vehicles: State of the art. *IEEE transactions on Vehicular Technology*, *59*(6), 2806-2814.
[18] Muthukumar, M., Rengarajan, N., Velliyangiri, B., Omprakas, M. A., Rohit, C. B., & Raja, U. K. (2021). The development of fuel cell electric vehicles–A review. *Materials Today: Proceedings*, *45*, 1181-1187.
[19] C. Armenta-Déu, J.P. Carriquiry and S. Guzmán (2019) Capacity correction factor for Li-ion Batteries: Influence of the Discharge Rate, Journal of Energy Storage, Volume 25, October 2019, 100839, DOI: https://doi.org/10.1016/j.est.2019.100839

[20] C. Armenta-Déu, J.P. Carriquiry (2020) aplication of Statistical Method to Determine Lithium Battery Capacity for Electric Vehicles, Journal of Automobile Engineering and Applications, Volume 7, Issue 2, pp. 25-35, doi: https://doi.org/10.37591/joaea.v7i2.4113

[21] C. Armenta-Déu (2021) Reduction of Electric Vehicle Driving Range due to Battery Capacity Fading, Journal of Automobile Engineering and Applications, Volume 8, Issue 2, doi: https://doi.org/10.37591/joaea.v8i2.6000

[22] Jin, Y., Zhao, W., Li, Z., Liu, B., & Wang, K. (2021). SOC estimation of lithium-ion battery considering the influence of discharge rate. *Energy Reports*, *7*, 1436-1446.

[23] Pay, S., & Baghzouz, Y. (2003, June). Effectiveness of battery-supercapacitor combination in electric vehicles. In *2003 IEEE Bologna Power Tech Conference Proceedings,* (Vol. 3, pp. 6-pp). IEEE.

[24] Oukkacha, I., Sarr, C. T., Camara, M. B., Dakyo, B., & Parédé, J. Y. (2021). Energetic Performances Booster for Electric Vehicle Applications Using Transient Power Control and Supercapacitors-Batteries/Fuel Cell. *Energies*, *14*(8), 2251.

[25] Kouchachvili, L., Yaïci, W., & Entchev, E. (2018). Hybrid battery/supercapacitor energy storage system for the electric vehicles. *Journal of Power Sources*, *374*, 237-248.

[26] Benmouiza, K., & Cheknane, A. (2018). Analysis of proton exchange membrane fuel cells voltage drops for different operating parameters. *International journal of hydrogen energy*, *43*(6), 3512-3519.

[27] Xu, Z., Qi, Z., He, C., & Kaufman, A. (2006). Combined activation methods for proton-exchange membrane fuel cells. *Journal of power sources*, *156*(2), 315-320.

[28] Van Der Linden, F., Pahon, E., Morando, S., & Bouquain, D. (2023). A review on the Proton-Exchange Membrane Fuel Cell break-in physical principles, activation procedures, and characterization methods. *Journal of Power Sources*, *575*, 233168.

[29] Qi, Z., & Kaufman, A. (2003). Quick and effective activation of proton-exchange membrane fuel cells. *Journal of power sources*, *114*(1), 21-31.

[30] Dey, T., Singdeo, D., Bose, M., Basu, R. N., & Ghosh, P. C. (2013). Study of contact resistance at the electrode–interconnect interfaces in planar type Solid Oxide Fuel Cells. *Journal of Power Sources*, *233*, 290-298.

[31] Chae, K. J., Choi, M., Ajayi, F. F., Park, W., Chang, I. S., & Kim, I. S. (2008). Mass transport through a proton exchange membrane (Nafion) in microbial fuel cells. *Energy & Fuels*, *22*(1), 169-176.

[32] Barbir, F. (2012). *PEM fuel cells: theory and practice*. Academic press.

[33] Halper, M. S., & Ellenbogen, J. C. (2006). Supercapacitors: A brief overview. *The MITRE Corporation, McLean, Virginia, USA*, *1*.

[34] Sharma, P., & Kumar, V. (2020). Current technology of supercapacitors: A review. *Journal of Electronic Materials*, *49*(6), 3520-3532.

[35] Jalal, N. I., Ibrahim, R. I., & Oudah, M. K. (2021, August). A review on Supercapacitors: Types and components. In *Journal of Physics: Conference Series* (Vol. 1973, No. 1, p. 012015). IOP Publishing.

[36] Banerjee, S., Sinha, P., Verma, K. D., Pal, T., De, B., Cherusseri, J., ... & Kar, K. K. (2020). Capacitor to supercapacitor. *Handbook of Nanocomposite Supercapacitor Materials I: Characteristics*, 53-89.

[37] Kadir, M. F. Z. (2021). Non-faradaic-based supercapacitor fabricated with fish skin gelatin biopolymer electrolyte. *Ionics*, *27*, 2219-2229.
[38] Arbizzani, C., Yu, Y., Li, J., Xiao, J., Xia, Y. Y., Yang, Y., ... & Passerini, S. (2020). Good practice guide for papers on supercapacitors and related hybrid capacitors for the Journal of Power Sources. *J. Power Sources*, *450*(227636.10), 1016.
[39] Conway, B. E., Birss, V., & Wojtowicz, J. (1997). The role and utilization of pseudocapacitance for energy storage by supercapacitors. *Journal of power sources*, *66*(1-2), 1-14.
[40] Barpanda, P., Fanchini, G., & Amatucci, G. G. (2008). Faradaic and Non-Faradaic Reaction Mechanisms in Carbon-iodine Nanocomposites Electrodes for Asymmetric Hybrid Supercapacitors. *ECS transactions*, *13*(17), 13.
[41] Sinha, P., & Kar, K. K. (2020). Introduction to supercapacitors. In *Handbook of Nanocomposite Supercapacitor Materials II: Performance* (pp. 1-28). Cham: Springer International Publishing.
[42] Mei Sam. Multiwalled carbon nanotubes based nanocomposites for supercapacitors. 325,
2006.
[43] Himadry Shekhar Das, Chee Wei Tan, and A. H.M. Yatim. Fuel cell hybrid electric vehicles: A review on power conditioning units and topologies. Renewable and Sustainable Energy Reviews, 76(February):268–291, 2017.
[44] https://en.wikipedia.org/wiki/Supercapacitor (accessed online: 17/06/2023)
[45] A. S. Samosir and A. H.M. Yatim. A novel control strategy of bidirectional dc-dc converter for interfacing ultracapacitor to fuel cell electric vehicles system based on dynamic evolution control. International Review of Electrical Engineering, 5(1):64–69, 2010.
[46] Julius Partridge and Dina Ibrahim Abouelamaimen. The role of supercapacitors in regenerative braking systems. Energies, 12(14), 2019.
[47] Hyundai NEXO breaks world distance record twice, https://www.hyundai.news/eu/articles/press-releases/hyundai-nexo-breaks-worlddistance-record-twice.html, accesso:03/01/2023, 2018.
[48] Ferrara, Alessandro, Jakubek, Stefan, Hametner, Christoph (2021). Energy management of heavy-duty fuel cell vehicles in real-world driving scenarios: Robust design of strategies to maximize the hydrogen economy and system lifetime. Energy Conversion and Management, 232:113795.
[49] Boretti, A. (2013) Analysis of the regenerative braking efficiency of a latest electric vehicle.
SAE Technical Papers, 12
[50] Kunz, M. R., Dufek, E. J., Yi, Z., Gering, K. L., Shirk, M. G., Smith, K., ... & Tanim, T. R. (2021). Early battery performance prediction for mixed use charging profiles using hierarchal machine learning. *Batteries & Supercaps*, *4*(7), 1186-1196.
[51] Ragone, M., Yurkiv, V., Ramasubramanian, A., Kashir, B., & Mashayek, F. (2021). Data driven estimation of electric vehicle battery state-of-charge informed by automotive simulations and multi-physics modeling. *Journal of Power Sources*, *483*, 229108.

[52] Toyota. Outline of the Mirai. Technical Report November, 2014. https://www.smartcirculair.com/wp-content/uploads/2020/06/Toyota-Mirai-FCV_Posters_LR.pdf

[53] Z. Cerovsky and Pavel Mindl. Regenerative braking by electric hybrid vehicles using super capacitor and power splitting generator. In 2005 European Conference on Power Electronics and Applications, volume 2005, pages 10 pp.–P.10. IEEE, 2005.

[54] Hydrogen Type 4 Cylinder 700 bar 51L, https://hyfindr.com/marketplace/components/hydrogentanks/ hydrogen-type-4-cylinder-700-bar-51l/, (accessed online: 15/11/2022)

[55] Hydrogen Type 4 Cylinder 700 bar 185L, https://hyfindr.com/marketplace/components/hydrogentanks/ hydrogen-type-4-cylinder-700-bar-185l/, (accessed online: 16/11/2022)

[56] EATON Electronics Division. XLM Supercapacitor 62 V and 69 V, 130 F Module, 2021.

[57] Armenta-Déu, C. and Cortés, H. (2022) Advance Method to Calculate Real Driving Range for Electric Vehicles, Journal of Automobile Engineering and Automation, Volume 9, Issue 3, pp.1-19, http://engineeringjournals.stmjournals.in/index.php/JoAEA/index

[58] Armenta-Déu, C. and Cattin, E. (2023) A new method to determine electric vehicle range I real driving conditions, International Journal of Vehicle Performance, Volume 9, Issue 1, pp.91-107, doi: https://doi.org/10.1504/IJVP.2023.10052227

[59] Armenta-Déu, C. and Cortés, H. (2023) Hybrid Method to Calculate Real Driving Range for Electric Vehicles in Urban Routes, Vehicles 5(2), 492-498, doi: https://doi.org/10.3390/vehicles5020027

[60] L. García-Arranz and C. Armenta-Déu (2021) Performance Tests to Determine Driving Range in Electric Vehicles, Journal of Mechatronics and Automation,
Volume 8, Issue 2, pages 10-20

[61] M. Hanako Olmedilla-Ishishi and C. Armenta-Déu (2020) Seasonal Variation of Electric Vehicles Autonomy: Application to AC/DC Dual Voltage Operation,
Journal of Mechatronics and Automation,b Volume 7, Issue 3 p.1-16,
doi: https://doi.org/10.37591/joma.v7i3.4489

[62] M. Martínez-Arriaga and C. Armenta-Déu (2020) Simulation of the Performance of Electric Vehicle Batteries Under Variable Driving Conditions, Journal of Automobile Engineering and Applications, Volume 7, Issue 3, pp.1-15, doi: https://doi.org/10.37591/joaea.v7i3.4448

[63] Zhifeng Que, Shixue Wang, and Weiyi Li. Potential of Energy Saving and Emission Reduction of Battery Electric Vehicles with Two Type of Drivetrains in China. Energy Procedia, 75:2892–2897, aug 2015.

[64] Sulaiman, N., Hannan, M. A., Mohamed, A., Majlan, E. H., & Daud, W. W. (2015). A review on energy management system for fuel cell hybrid electric vehicle: Issues and challenges. Renewable and Sustainable Energy Reviews, 52, 802-814.

[65] Wu, Y., & Gao, H. (2006). Optimization of fuel cell and supercapacitor for fuel-cell electric vehicles. *IEEE transactions on Vehicular Technology*, *55*(6), 1748-1755.

 doi:10.20944/preprints202306.1466.v1